Provision of Power Oscillation Damping from Wind Power Plants

Mads Due Riis

Wind Power Systems, WPS4-1054, 2023

Master Thesis

STUDENT REPORT

AALBORG UNIVERSITY

AAU Energy
Aalborg University
http://www.aau.dk

AALBORG UNIVERSITY
STUDENT REPORT

Title:
Provision of Power Oscillation Damping from Wind Power Plants

Theme:
Power oscillation damping functionality from wind power plants.

Project Period:
Spring Semester 2023

Project Group:
WPS4-1054

Participant(s):
Mads Due Riis

Supervisor(s):
- Florin Iov

Page Numbers: 44

Date of Completion:
September 4, 2023

Abstract:

This thesis develops a design strategy for power oscillation damping (POD) control from a wind power plant (WPP) perspective to enhance power system small signal stability. As the WPP operators usually only have measurement access to the point of common coupling (PCC), the analysis uses a simple grid model to minimize the impact of the surrounding power flow in the results. The design tackles phase shift correction related to measurement delay, variable communication delay and wind turbine (WTG) response time. The strategy of the POD control design uses seven parallel branches of band-pass filters and lead regulators in order to divide the defined frequency range into smaller ranges to correctly compensate for the frequency dependent phase shifts in the system. With the assumed time responses of the analysed system, the designed controller is able to produce reactive power with opposite phase of the voltage at PCC with acceptable precision.

Nomenclature

Abbreviation	Description
AVR	Automatic Voltage Regulator
BP	Band-pass filter
HP	High-pass filter / Washout filter
LP	Low-pass filter
PCC	Point of Common Coupling
PoC	Point of Connection
POD	Power Oscillation Damping
POD-P	Power Oscillation Damping with active power
POD-Q	Power Oscillation Damping with reactive power
PO-range	Power oscillation range (0.1-2.0 Hz)
PPC	Power Plant Controller
PPO	Power Plant Operator
PSS	Power System Stabilizer
PU	Per Unit
SCR	Short Circuit Ratio
TSO	Transmission System Operator
X/R	Reactance/Resistance
WPP	Wind Power Plant
WTG	Wind Turbine Generator

Contents

1. Introduction

1.1 Background and motivation

1.1.1 History of power oscillations in power systems

Low frequency power oscillations have always been an issue in power system stability, but the issues grew in the 1960's, where automatic voltage regulators (AVR) were introduced to most synchronous generators [1]. Power oscillations in a power system are caused when generators or sets of generators oscillate against each other. If the damping in the power system is insufficient, it can lead to voltage fluctuations, frequency fluctuations, equipment damage and in worst case the instability can lead to a black out of the power system [2].
Power oscillations (or low frequency power oscillations) are divided into four different modes [3]. These modes are characterized by identifying which generators are "hunting" which.

- Intraplant mode (2-3 Hz). Oscillations between generators inside a single power plant.
- Local mode (0.8-1.6 Hz). Oscillations between a single generator or power plant against a large power system.
- Inter-area mode (0.1-0.7 Hz). When the power system or part of it is split into two (or more) groups oscillating against each other.
- Exciter mode (1.5-2.5 Hz). Oscillations within the excitation system usually due to poorly tuned stabilizers.

A recent example of the consequences of power oscillations occurred in February 2011 in the Continental European power system [4]. Generators in the southern part of the grid (Italy) were swinging with a frequency of 0.25 Hz against the northern part of the grid. This resulted in power swings of 150 MW over tie lines and voltage swings of $\pm$ 5 kV on the 400 kV system. In European terms this is known as a North-South inter-area mode.
In December 2016 inter-area power oscillations were observed on the west-east axis, from Spain to Turkey with oscillations of 0.15 Hz. The oscillations were characterised as a three area oscillation called west-center-east mode as oscillations were observed in all three areas with different phases [5].
Another event was observed in December 2017 with an oscillation frequency of 0.29 Hz [6] and voltage swings of up to $\pm$ 10 kV. This was also a north-south oscillation where generators in southern Italy oscillated against northern part of the grid. However, since the oscillation contribution

from northern-central part of the grid was limited, this event was characterised as a local mode as generators in the south of Italy where oscillating against the rest of the CE grid.
The frequency ranges suggested by [3] from 1993 are based on observations of the power system at that time. The observations in 2017 contradict these ranges and concludes that they are not valid in a modern power system with higher penetration of renewable energy. Instead power oscillation modes are defined by their origin rather than the particular frequency range.

1.1.2 Power oscillation damping in power systems

The main provider of damping in the power system is the Power System Stabiliser (PSS) which every large synchronous generating unit is equipped with. The PSS adjusts the excitation of the synchronous machine, usually based on the rotational speed, to counteract oscillations in the system. The PSS is designed with a gain, a washout filter and a phase compensation block as seen in Figure 1.1. The washout filter filters out low frequency signal while the phase compensation ensures that the phase lag between the exciter input and the output torque is correctly compensated. Two consecutive phase compensation blocks are often needed to provide sufficient amount of compensation. For a perfectly compensated PSS, the phase characteristic output of the PSS would be exactly opposite to the phase characteristics desired to damp [7].

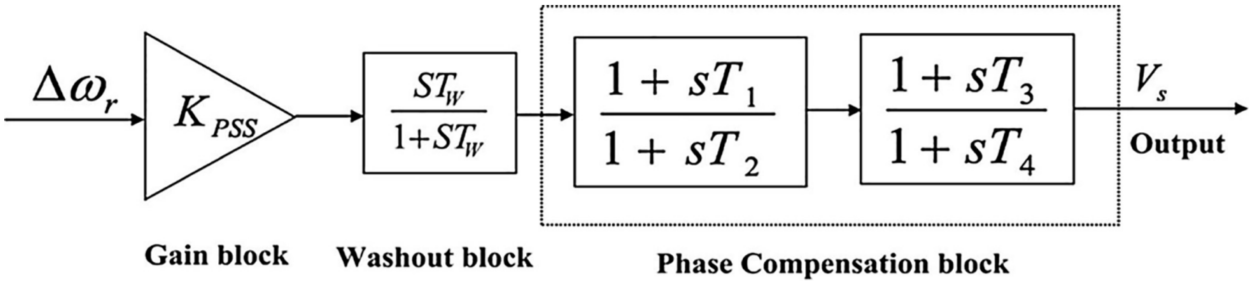

Figure 1.1: Block diagram representation of a classical Power System Stabilizer (PSS) [8]

1.2 State of the art on power oscillation damping by WPP

1.2.1 Existing grid codes

As power oscillation damping functionalities from WPPs are still a new technology, the requirements from system operators around the world are still very limited. In general there are multiple grid codes where power oscillations are touched upon in regards to limiting the power oscillations produced by the WPP. ENTSOE-E specifies [9] that power generating units are not allowed to adversely affect the power oscillation damping capabilities thereby targeting the power oscillations

inside the plant (Intraplant mode) and the oscillations from the plant against the grid (Local mode). The grid codes currently in development by the danish TSO, i.e. Energinet, suggests a limit for power oscillations produced by the power plant at ± 0.5 % of produced power and ± 0.25 % of the nominal power of the plant [10].
To the best of the authors knowledge, there are no specific limits in any grid codes at the moment regarding the contribution to damping capabilities of oscillations generated outside the plant. In countries such as Sweden and Saudi Arabia grid codes state that a POD function is needed but does not specify the amount of damping required by connected generators. In e.g. Sweden, grid codes [11] states that type C and D generating plants (from ENTSO-E definitions) must have POD functions and contribute to damping of oscillations in the frequency range of 0.25 Hz - 1 Hz.

1.2.2 Previous studies

To research how the damping contributed from a WPP POD controller can affect the power oscillation in a larger power system the author of [1] developed a 12-bus system divided into four areas of different characteristics. State-space and eigenvalue analysis are used to determine the observability and controllability of both active and reactive POD on the 12 busbars. On top of this a Prony analysis is conducted to further analyse the oscillatory system behavior. It is shown that wide area measurements as input will cause better damping capabilities than local measurements. These in depth analysis give the best understanding of where to measure small signal stability and also where to act on a particular power oscillation event. However, from a power plant developer point of view this approach would mean an extensive amount of grid data and modelling of the grid surrounding the PCC. This might be possible for island grids where the size of the grid is limited, but cause serious issues with large systems as inter-area oscillations oscillate over very large areas. Furthermore, it requires that the plant operator has both measurement rights and ability on selected busbars in the grid.

In [12] engineers from Vestas discuss some of the theoretical and practical challenges of a power oscillation function from a wind power plant perspective. As active power production is directly dependent on the variable wind speed, the plant must operate at a sub optimal level in order to have the capabilities of reliable contribution with active power damping (POD-P). Further challenges of POD-P include mechanical eigenmodes of the tower and blades because extracting an oscillation of active power means an oscillation in load on the generator which in turn can cause the mechanical structures to oscillate if the frequency of the PO is close to the eigenfrequencies of the structures. On the other hand, power oscillation utilizing reactive power control (POD-Q) have implications with voltage control functions used in WPP power plant controllers (PPC). Based on the 12-bus system of [1], it is shown how the optimal phase angle of the generated counter oscillation varies for different locations in the system for damping with both active and reactive power. The paper suggests an exception to the voltage-slope grid requirements used in most countries when power oscillations are detected. This exception should allow the power plant to have a higher rise time than 1 second for a given period (e.g. 1 minute) while damping the oscillations before returning to the usual 1 second rise time requirement.

Several advanced studies has been carried out on observability of power oscillations in power systems. These studies use different power system models as a 12-bus system [1, 12] or IEEEs 68-bus system [13, 14] to analyse the observability and controllability of the given system and utilize this to tune POD controllers. Consequently, the studies are based on the power system representation being studied. The objective of such analysis is to determine in which busses power oscillation damping functionalities will have the biggest impact on the overall system stability. Utilizing this information can identify where damping frequencies should be injected and whether active of reactive power modulation would be most efficient for any given oscillation. However, as power system comes with large variance, results of these analysis may not be valid for all existing and future power plants being installed by power plant operators (PPO).

1.3 Problem Statement

As the green transition of energy production increases the amount of renewable production and decreases the share of classical synchronous generators in power systems, renewable sources must also take on the responsibility of system stability. The small signal stability responsibility has been on power system stabilizers connected to large synchronous generators, but as converter technology improves, WPP with variable speed turbines have capabilities to also contribute to the overall damping capabilities.
This project aims to investigate and propose power oscillation damping functionality from wind power plants to increase the small signal system stability. The proposed POD controller aims to cover a wide range of frequencies for the power oscillations that may occur on the electricity grid. The design and tuning of the POD controller will tackle the challenge of delayed measurements and variable communication delays for a representative wind park including external grid. The proposed design will be verified through simulation studies under different operational conditions. From the perspective of wind power plant operator it is very complicated to simulate the amount of damping capabilities of a power oscillation damping function because it depends on the topology of the connected grid. If such functionality in wind power plants should be implemented on a large scale complete modelling of power systems require extensive research and simulation time. By solely looking at the point of connection, this project aims to design robust tuning for POD controllers based on a system more generally applicable.

1.4 Scope

The goal of this thesis is to provide a standardised analysis of power oscillation damping from the perspective of a wind power plant operator. The POD design methodology established in this thesis simplifies the grid to a Thevenin equivalent external grid so the analysis and results will be applicable for PPOs throughout their different locations. The power plant controller will measure and act on the PCC, hence voltage is the best parameter to measure for power oscillation detection. This is because current, and thereby power, measurements on the connection bus can be misleading when there is no knowledge of the direction of currents from the bus towards adjacent busses.
The power oscillations will be damped with the use of parallel POD controllers to cover the typical range of power oscillations of 0.1 Hz to 2 Hz. With parallel controllers, the goal is to achieve sufficient damping of precise oscillations without affecting the whole range.

Delimitations The actual damping capabilities of the POD controller designed will not be tested in this project. Both observability and controllability of power oscillations depends on the grid topology, hence any testing of this will be based on several assumptions as the full grid topology is too extensive to model. The final damping capabilities of a developed POD controller can only really be tested when it is implemented in the physical system. This is also reflected in the grid codes presented in section 1.2.1, where even the most updated ones only require that a power oscillation damping function is available.

2. System Characterization

This section gives an overview of the system in which the developed controller will be tested. To determine the best system for this particular project a set of requirements are presented. The requirements are based upon the scope and goals of the project defined in section 1.4.

System Requirements:

- Grid representation must be general - So the analysis and thereby results are not dependent on the grid topology.
- Grid representation should be able to produce specific oscillations between 0.1 and 2.0 Hz.
- WPP with multiple turbines to facilitate variable communication delay.
- WPP with different feeder lengths to turbines so the voltage level on the WTG terminals vary.
- Small and scalable WPP model.
- Introduction of measurement delay.

2.1 Grid representation

A very simple grid connection representation is the Thevenin equivalent with a ideal voltage source behind a configurable series impedance. A similar approach will be used in this system. However, the voltage source will not be just a steady ideal voltage source as it will be used to simulate power oscillations within a defined frequency range. With this representation it is possible to inject specific power oscillation frequencies to the point of common coupling through the grid impedance. Since the POD-functionality in scope of this project is only interested in the behavior at the PCC, a simple representation like this is sufficient. Since the PPC is the only busbar available for both measurements and power injection, the results can be applicable for all power systems as long as both measurements and power injection are on the PPC.

2.2 Wind Power Plant representation

A wind power plant topology consisting of two feeders with nine turbines on each is designed for this project. This is a scaled down representation of offshore plants which typically has several feeders. The voltage level of the two feeders and the turbines is 33 kV which transforms to 150

kV through the park transformer before reaching the point of common coupling (PCC). In most offshore wind power plants a transport cable of several kilometers would connect to the shoreline where another transformer (e.g. 150kV/400kV) would transform the voltage even higher before connecting to the high voltage grid. In cases like this the PCC would be situated after the transport cable. Since this project aims to make a general analysis for both onshore and offshore this extra complexity is not included in the system setup.
Figure 2.1 illustrates how the turbines on each feeder are connected in series. This means the current from the turbines are accumulating and cause large differences in current throughout the feeder. The cables on the beginning of the feeder (between bus 3, 4 and 5 ..) are dimensioned for larger currents and thereby greater cross section compared to the cables between the busses further down the chain.

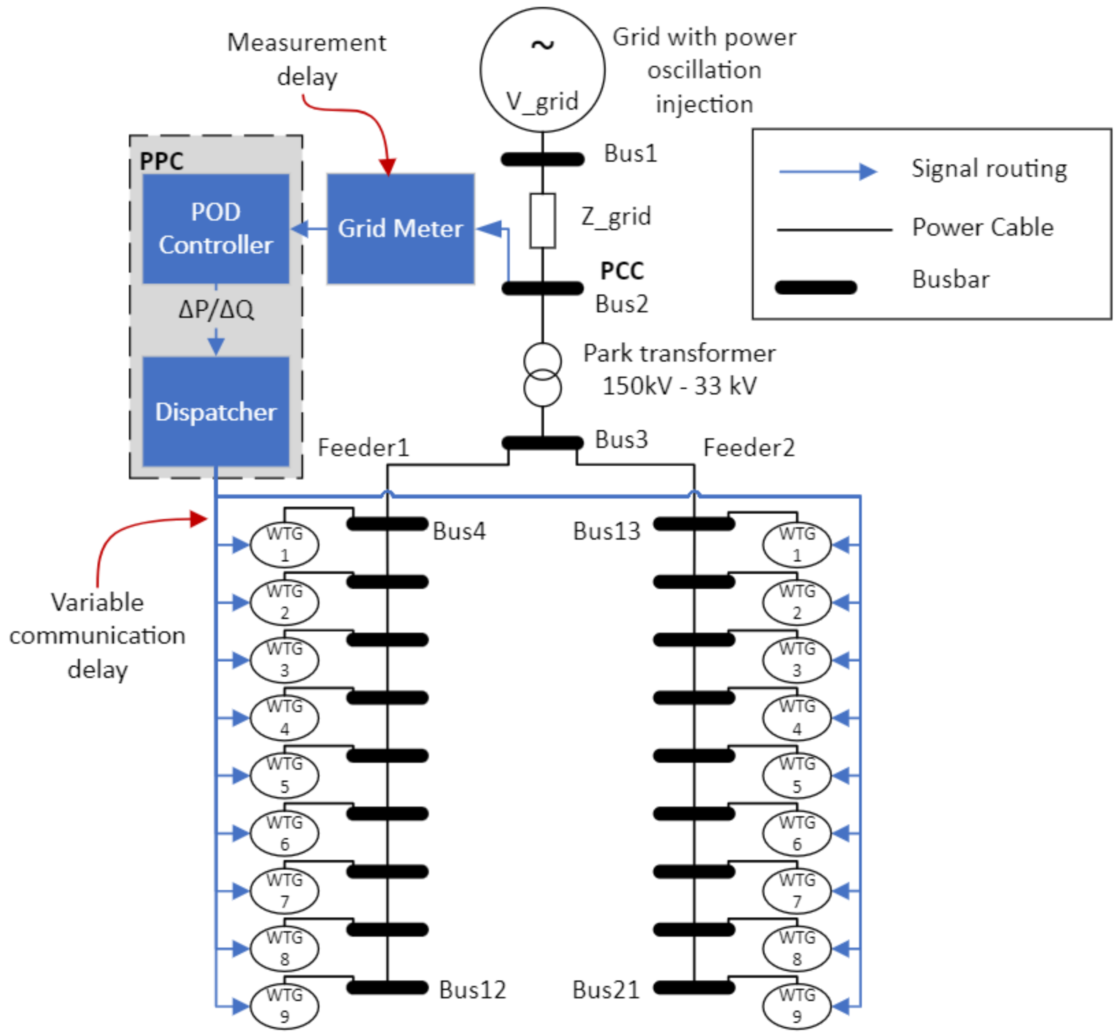

Figure 2.1: System topology. WPP layout, grid representation and signal routing for measurement and control

2.3 Data signal processing

A real measurement of power system values will always introduce some delay to the system due to the transformation from analog measurement to digital input to the PPC as well as communication time from the measurement device. The Grid Meter block in Figure 2.1 represents the delay related to the measurements.
Grid meters available on the market [15, 16, 17] has been found to have a measurement delay time between 3.3 to 20 ms for voltage and current measurements. For frequency measurements the time delay is between 10 to 20 ms. For the sake of this project a measurement delay of $T_{D.meas} = 10$ ms will be assumed when measuring the voltage.

Communication from power plant controller (PPC) to all connected WTGs can be done in numerous ways depending on the plant layout. For an array based layout as presented in Figure 2.1 one communication strategy is the hop-by-hop manner. With this strategy the communication is passed from the PPC to a whole array at once. The signal is sent to the first WTG which reads the signal, acts on it, writes feedbacks to the signal and then sends it to the next turbine [18]. To analyse the time delays to each turbine the two factors, internal WTG delay and transport delays between turbines, need to be estimated. In [19] the authors estimate the internal delay in the wind turbine controller to 1.1 ms and 0.098 ms depending on hardware bandwidth, through a simulation setup. As the internal delay depends on the sensor and controller hardware, amount of passed data etc. this project will adapt the conservative estimation as found by simulating with the slower communication speed, $T_{D.WTG} = 1.1ms$.
The transport delay is discussed and also simulated in [19] where it was found to be in the area 11.87-13.06 ms for 100 Mbps channel speed and 1.16-1.28 ms for 1 Gbps. Due to the author's insights of power plant control design at Vestas, the faster range is chosen and the delay is set to $T_{D.transport} = 1.2$ ms. However, it should be noted that using a 10 times higher transport delay will cause very significant changes to the total delay of the furthest turbines.
Figure 2.2 shows that the communication delay with the hop-by-hop concept accumulates and delays are added over both distance and amount of turbines.

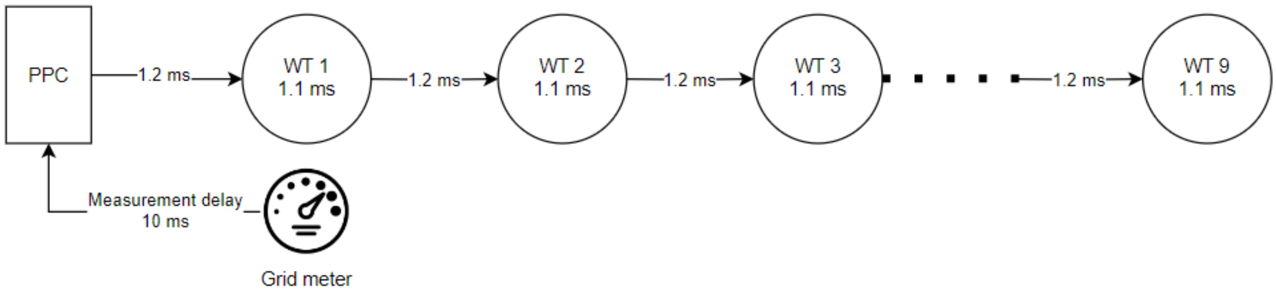

Figure 2.2: Diagram of the communication strategy showing the delays accumulate for the furthest turbines

The total delay for each turbine is then found by

$$T_{D.tot.n} = T_{D.meas} + n(T_{D.WTG} + T_{D.transport}) \tag{2.1}$$

where n is the turbine number for each array. The variance in delay caused by communication is 2.3-20.7 ms, causing the maximum total delay to be $T_{D.tot.n} = 30.7$ms.

2.4 Summary

The system characterization is based on a set of requirements created to ensure that the developed system fits the project scope. The grid is represented by a Thevenin equivalent voltage source since the requirement dictates a very simple and general grid representation. The voltage source is however not a constant 1 pu, as it is used to generate power oscillations within the range of 0.1-2.0 Hz. The wind power plant consists of 18 turbines connected on two feeders of nine turbines each. The two feeders are connected to the low voltage side of a park transformer which transforms the voltage from 33 kV to 150 kV and connects to the PCC. The PCC voltage is measured by a grid meter with a measurement delay of 10 ms. The communication strategy hop-by-hop is applied, where the total delay depends on the transport time of the signal between turbines and the internal WTG processing time. The internal processing delay is estimated to 1.1 ms, and the transport time to 1.2 ms. As the the hop-by-hop strategy defines, the signals are passed to the first turbine and then from turbine to turbine causing the delay to be in the range of 2.3-20.7 ms.

3. Model design

3.1 WTG model

The WTG model used in this analysis is a full scale converter WTG, i.e. type 4. Turbines using the full scale conversion are widely used throughout power systems along with the double fed induction generator of type 3. The analysis will be based on a 3.6 MW turbine with a wingspan of 120 meters as the Siemens SWT-3.6-120.
In [20] a performance model for hybrid power plants including a wind turbine model is proposed and validated against two turbines. The model interprets the WTG response as a first order system and includes random wind generation as well as the inertia. Since no converter, generator or blade dynamics are analysed in this thesis, a simple representation like the first order response is sufficient.
The continuous transfer function of a first order system is showed in (3.1).

$$\frac{1}{\tau_{WTG} \cdot s + 1} \tag{3.1}$$

The speed of the wind turbine response is determined by the time constant τ_{WTG} which is defined as

$$\tau_{WTG} = \frac{1}{2 * \pi * f_0} \tag{3.2}$$

where f_0 is the bandwidth of the turbine. As defined by equation (3.2) the time constant decreases when the bandwidth increases reflecting that faster turbines will have faster time response.
Since the response of the WTG is not instant it introduces a phase-lag on sinusoidal inputs that needs to be compensated by the controller in order to provide the correct output phase. The phase-lag, ϕ, of a first order system depends on τ_{WTG} and the input frequency, ω as

$$\phi_{WTG} = \tan^{-1}(\omega \tau_{WTG}) \tag{3.3}$$

The magnitude or damping of the first order response is the magnitude of equation (3.1) with s replaced by $j * \omega$

$$\zeta_{WTG} = \left| \frac{1}{\tau_{WTG} \cdot j \cdot \omega + 1} \right| \tag{3.4}$$

In the performance model the value of τ_{WTG} is set at 0.25 for Q response. In Figure 3.1 this value is plotted in a Bode diagram against two other values. It is visible, that both damping and phase shift from the turbine depends highly on the response speed. Slower responding turbines can cause issues since lead-regulators with high gain and phase shift are needed to compensate. For this project f_0 is set to 1 Hz which according to equation (3.2) corresponds to $\tau_{WTG} = 0.159$. Note that with a faster WTG response of 10 Hz bandwidth, the magnitude becomes neglectable in the frequency area of interest. The phase shift becomes significantly lower and is only at around 10 °at 2 Hz. This shows that faster responding turbines simplifies the POD controller drastically.

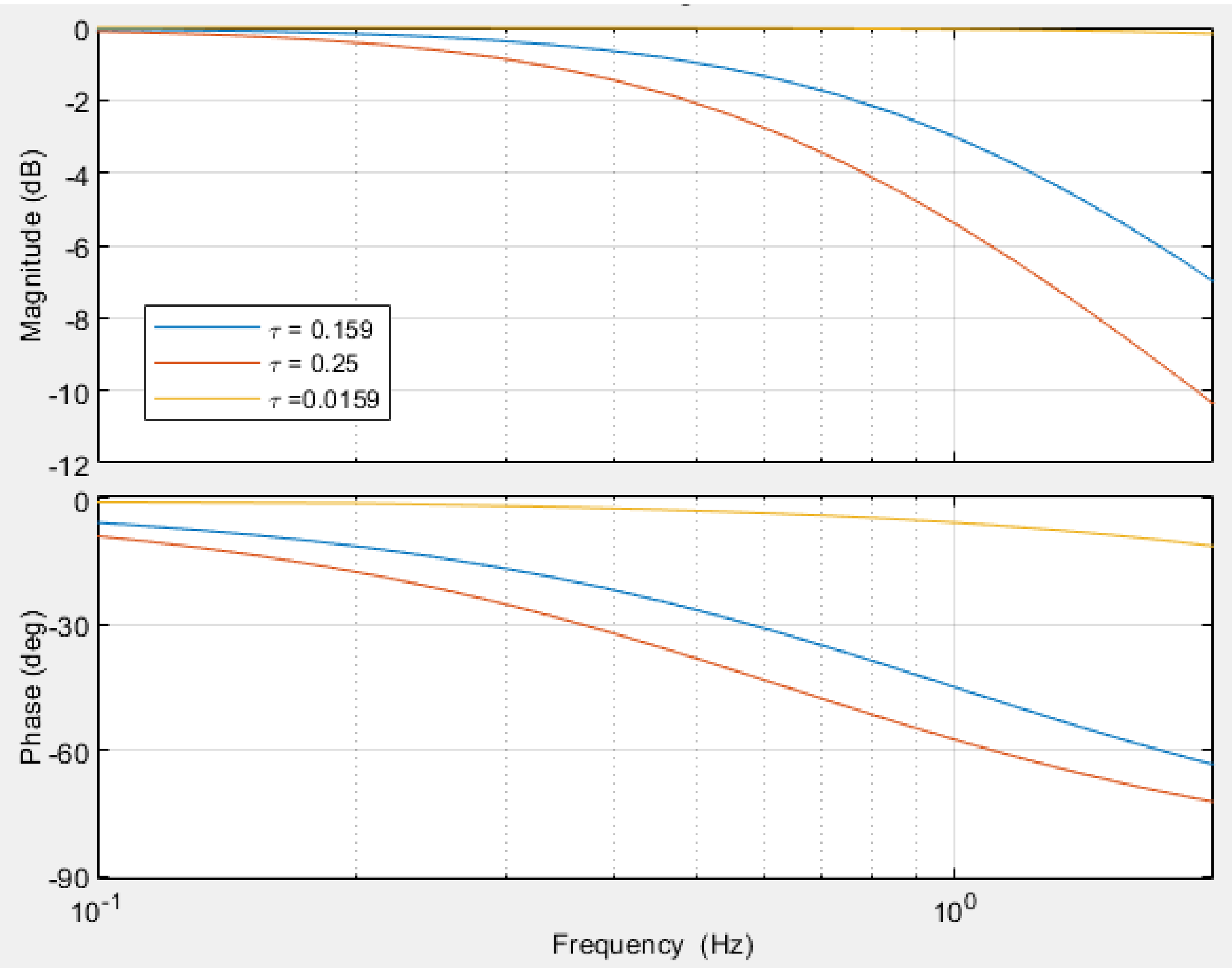

Figure 3.1: Bode plot of WTG response in the frequency area of interest for three different values of τ. The clue curve of $\tau = 0.159$ is used for this project.

The reactive power capabilities of the WTG used in the model are $\pm$ 0.33 p.u. independent of active power output [20] as shown in Figure 3.2.

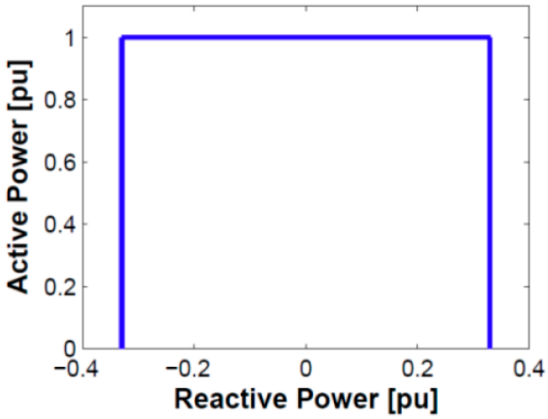

Figure 3.2: Reprint of PQ diagram from [20] showing the reactive power capability of the WTGs in p.u.

3.2 Transformer and cables

The system topology in Figure 2.1 showed the cable setup for the wind power plant with two identical feeders each connecting nine turbines in series. Due to the series connection it is obvious that the current through the feeder will not be constant. For efficient cable design, the cables must increase in size as the current does closer to the collector bus.

The cable distance between turbines is dictated by the optimum spacing of wind turbines with respect to both cost and aerodynamic losses. For minimizing the aerodynamic losses a distance of $10D - 15D$, where D is the rotor diameter is considered good practice for offshore wind power plants. However, with the rotor diameters of modern turbines increasing, the cost of power cables is so significant that a lower range of $6D - 10D$ is often used for modern plants [21]. Based on these practices, the distance between turbines for this project is selected as $10D$. Using $D = 120$ m as defined in this project, the cable length between turbines will be 1200 m.
The cables are modelled using the nominal π model [22] with the parameters R as resistance, X as reactance and B as shielding susceptance as illustrated in Figure 3.3

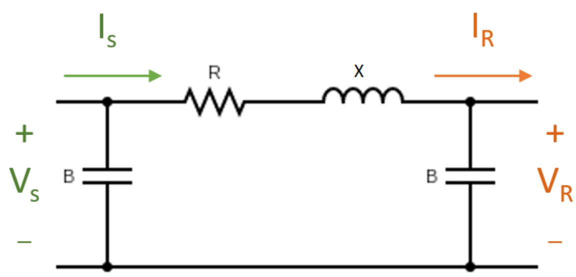

Figure 3.3: π model representation of cables in the wind power plant

The size of the cables is determined by the maximum passing current from the wind turbines when voltage is at the lowest allowed point (0.9 PU) which is calculated as

$$I_{wtg.max} = \frac{\sqrt{P_{nom}^2 + Q_{nom}^2}}{0.9 \cdot V_{nom} \cdot \sqrt{3}} \tag{3.5}$$

where Q_{nom} is $0.33 \cdot P_{nom}$ as defined in section 3.1. As the turbines in each array are connected in series the maximum current through the cable is defined as

$$I_{cable.max_N} = I_{wtg.max} + I_{cable.max_{N-1}} \tag{3.6}$$

From the maximum current in each of the array lines, the cables are defined from ABB's XLPE submarine cable catalogue [23]. Table A.1 in the Appendix shows the maximum current and the corresponding cable current and cross section.

The park transformer is modelled as the equivalent circuit of Figure 3.4 with R_{eq} and X_{eq} being, respectively the resistance and reactance of the transformer windings on both sides of the transformation. This model is neglecting the magnetization branch of the shunt connected resistor and inductor. This is a simplification frequently done [22] [24] since the magnetization current in large power system transformers is often less than 5 % of the rated current [24]. This simplification can be justified since the performance of the transformer is not studied during this project. As the model utilizes the Per-Unit system also the winding ratio is omitted. No tap-changer is used since the studies does not evolve around voltage stability studies. Specific values for R_{eq} and X_{eq} are calculated from parameters of a transformer with rated power of 120 MVA [25] and can be seen in Appendix A.

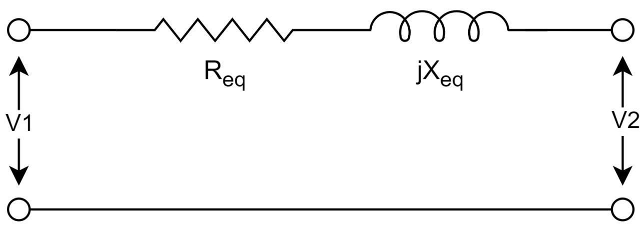

Figure 3.4: Transformer equivalent circuit neglecting magnetization branch and winding ratio.

3.3 Grid model

The grid is modelled as a Thevenin equivalent voltage source. For the studies in this project the grid is assumed to have high stiffness with a short circuit ratio (SCR) of 30 and reactance-to-resistance ratio (X/R) of 10 as seen from the PCC. With the equations (3.7) and (3.8) the resistance and reactance are calculated.

$$Z_{grid} = \frac{V^2}{S_B \cdot SCR} \tag{3.7}$$

$$Z_{grid}^2 = R_{grid}^2 + X_{grid}^2 \tag{3.8}$$

Power oscillations are created on the grid with ideal sinusoidal signal inputs on the voltage at the the grid bus. The amplitude and frequency is thereby easily controlled to test the WPP as a POD device on different power oscillation events.

3.4 Delay handling

Both the measurement and communication delays are represented by a continuous delay where the magnitude is indifferent and the phase shift is

$$\phi_{Delay} = T_{Delay} \cdot \omega \tag{3.9}$$

where $T_{Delay} = n(T_{D.WTG} + T_{D.transport})$ for the communication delay as per (2.1) and $T_{Delay} = T_{D.Meas}$ regarding measurements. The maximum phase shift due to communication delay is found at the ninth turbine when damping an oscillation at 2 Hz. In this case $\phi_{Delay} = 14.9°$.

3.5 Summary

The turbine model is based on a turbine like the Siemens Gamesa SWT-3.6-120 using full scale converter (type 4) with a 3.6 MW generator and a wingspan of 120 m. The WTGs are modelled as first order responses where the turbine bandwidth of 1 Hz dictates the the speed of the response. In order to adequately control design later, the phase shift and damping of the first order response is researched through bode diagrams of different response speeds. The reactive capabilities used for the turbines is $\pm$ 0.33 p.u. independent of the active power output.
Cables between WTG busbars and the collector bus are modelled using the π model. The length of the cables are estimated to be 10 times the turbine diameter, 1200 m. As the turbines in each array are connected in series the cables are designed for higher currents closer to the collector bus. This design is based on the maximum current through the cables with maximum active and reactive power produced in at time of minimum allowed voltage. The park transformer is modelled by neglecting the magnetization branch and represented by a resistance and reactance. As PU system is utilized in the model, the winding ratio is without impact.
The Thevinin equivalent grid representation is modelled as a stiff grid with a SCR of 30 and X/R-ratio of 10 as seen from the PCC.
By using the estimations defined in Chapter 2, the maximum phase shift is identified to be 14.9°.

4. Control System Design

The POD controller is tuned with a simple system where the all the WTGs are lumped together as one power plant acting directly on the PCC. This means cables, transformer and communication delay all are omitted for now. The open loop control system as shown in Figure 4.1 is used to check if the POD controller can compensate for the phase shift introduced by the WTG response and the measurement delay. The goal of the open loop control is to control the output of the WTG to have a similar frequency and magnitude, but with opposite phase to the input oscillation. Since a negative unit gain will shift the phase 180°, the design presented in this chapter will simply aim to achieve the same phase characteristics rather than the opposite, in order to ease the visibility of plots.

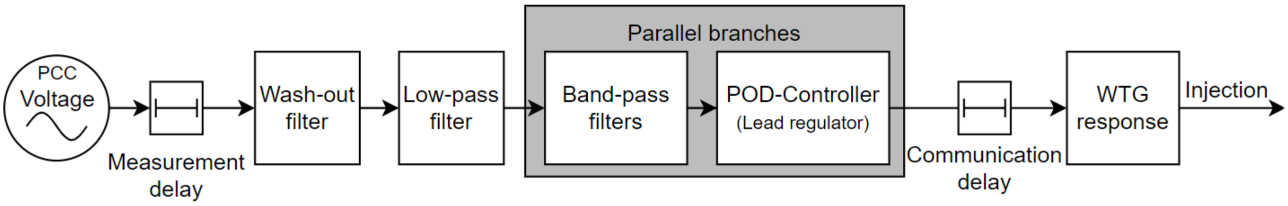

Figure 4.1: Block diagram of the open loop control system.

4.1 Filter design

Initially a wash out filter eliminates the low frequency signals below the interested area and a low pass filter to eliminate frequency higher than the typical PO-range. This ensures that the POD-controller will only act on oscillations where it is expected to. These filters are designed rather conservative to avoid impacting the phase characteristics inside the PO-range. The filters shown in Figure 4.2 are designed with cutoff frequencies $\omega_{LP} = 0.01$ and $\omega_{HP} = 20$, which is a factor of 10 away from the PO-range. As visible the damping inside the range is neglectable and the phase shift is kept under 5°.

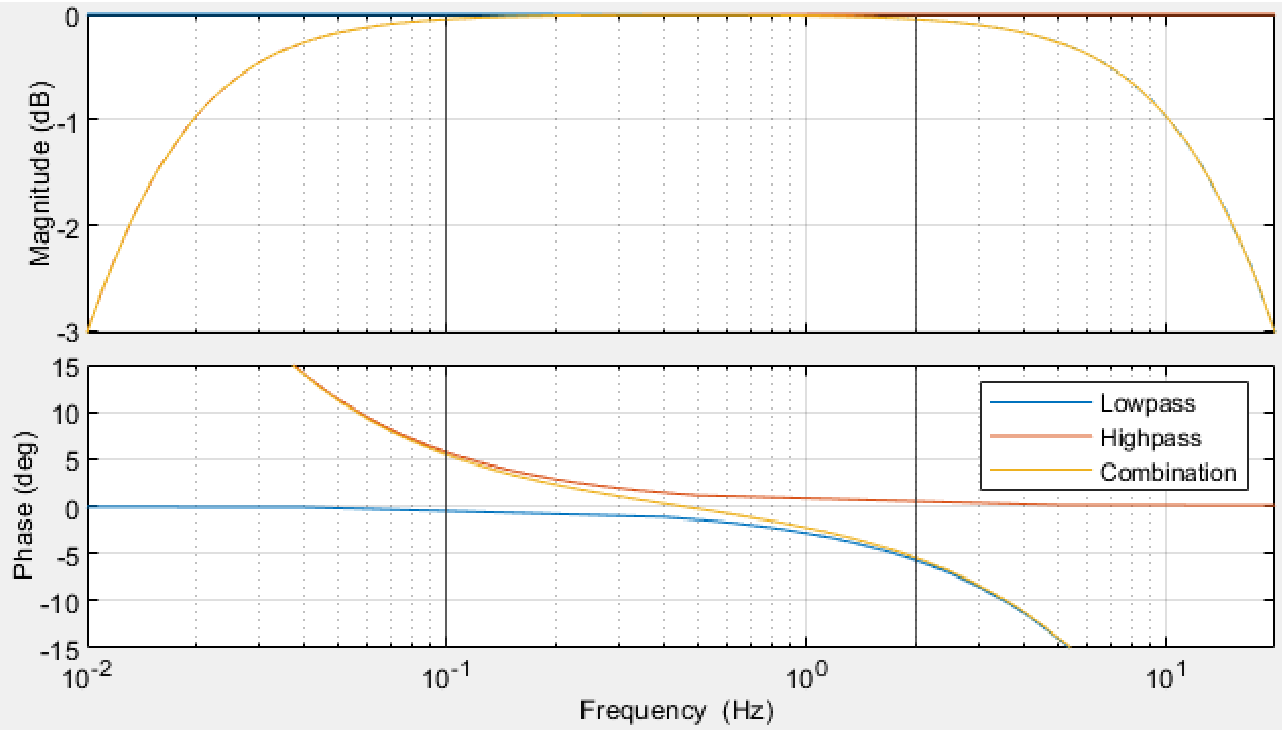

Figure 4.2: Bode diagram of the high and low pass filters and their combined phase characteristics. Black vertical lines show the PO-range.

To increase the performance of the overall control, the power oscillation range (0.1-2.0 Hz) is handled by several parallel band-pass filters and controllers. This strategy is also known from synchronous generator connected multi-band power system stabilizers (MB-PSS), where the oscillation range is divided into narrow ranges to strengthen the overall damping capabilities. The band-pass filters are designed using (4.1)

$$H(s) = \frac{s \cdot H_0 \cdot \omega^2}{s^2 \cdot \dfrac{\omega}{Q} s \cdot \omega^2} \tag{4.1}$$

where $H_0 = \dfrac{1}{Q}$ is the gain, and Q is the quality factor determining the steepness band [26]. The higher the value of Q, the more narrow the band-pass filter is. Figure 4.3 shows five band-pass filters designed with a quality factor of 2 being logarithmic evenly spread throughout the PO-range. Each filter has a gain of 0 dB and 0 °phase shift at the design frequency. With the five-filter-design the filters overlap their neighbouring filter at -4 dB and phase shift around 50°.

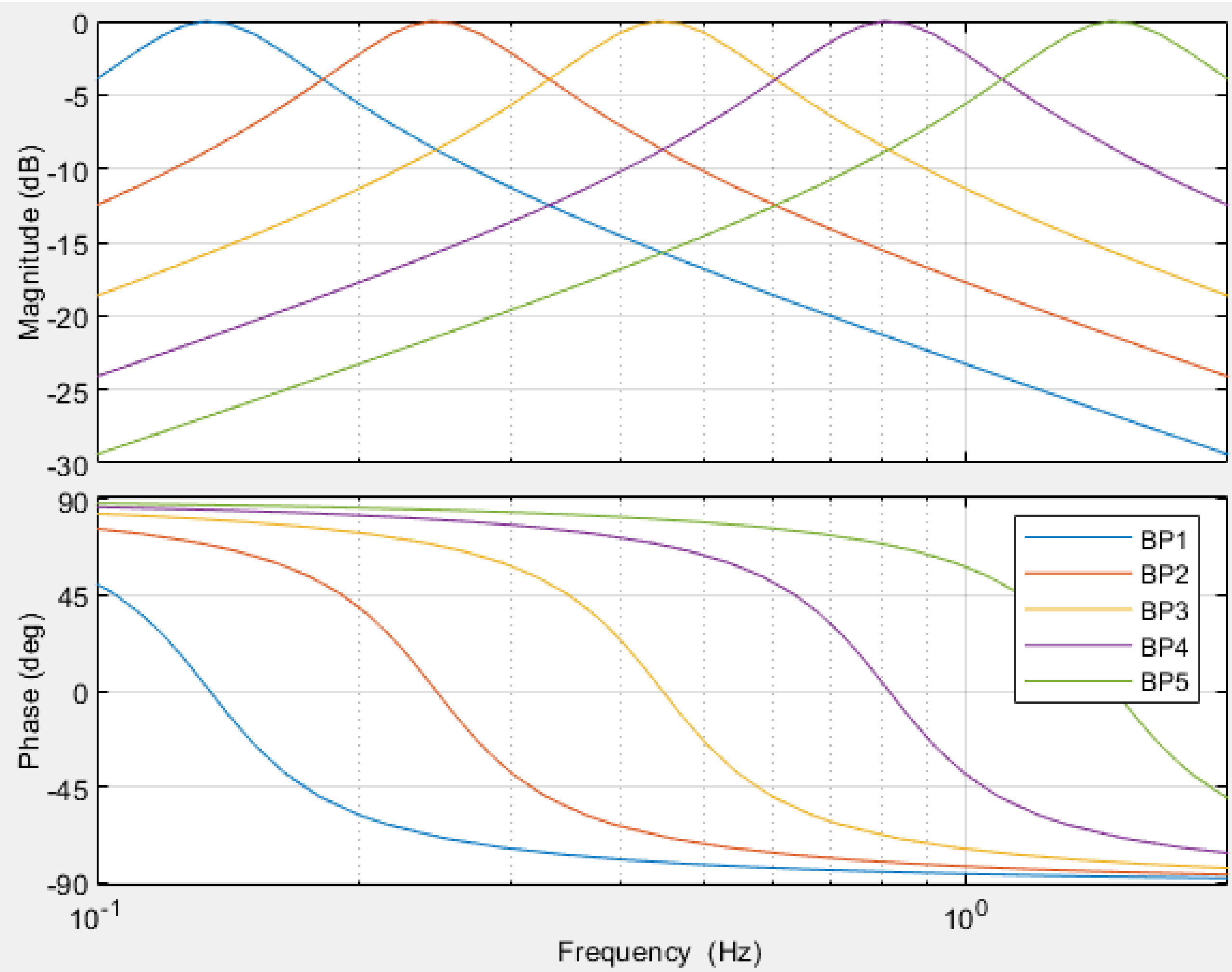

Figure 4.3: Bode plot of the five parallel band-pass filters. The x-axis is showing the full operating range from 0.1-2.0 Hz

Controller outputs should be added together to act as the POD output, with this in mind, the output of only the parallel filters are added together to investigate their impact. In Figure 4.4 the response of the band-pass filters and their summation is seen compared to the input signal with 0.5 Hz frequency.

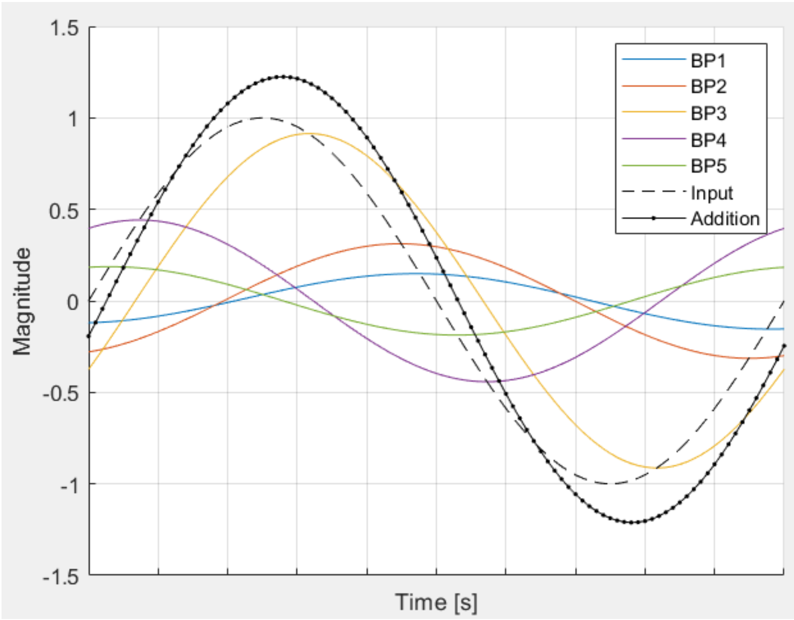

Figure 4.4: Response plot of the band-pass filters with an input signal of 0.5 Hz.

The addition signal, which is the sum of all band-pass outputs, is leading the input signal and also have a higher amplitude. Further investigation on multiple input frequencies showed that for all signals above the design frequency for band-pass 3 (the central filter, 0.45 Hz) the output will be leading the input. Similarly, for the signals below this frequency the output is lagging. Moreover, the gain varies with the frequency of the input signal as shown by the blue curve in Figure 4.5. Even though some variance in gain can be expected this behaviour will cause issues. These issues are consequences of the middle band-pass filter having more neighbouring filters to each side than the boundary filters. By looking at the initial Bode plot in Figure 4.3 it is clear that the sum of gains is higher for oscillations in the middle of the spectrum.

Two possible solutions to this uneven gain and phase characteristics are; 1) include filters for a much wider range than the PO-range or, 2) adjust the gain of each filter. The first solution would require many filters designed outside the PO-range, which could be affected by the low-pass and washout filters placed before the band-pass filters. However, the second solution alone will not sufficiently adjust the lower gains before the first design frequency and after the last. A suggestion for mitigating this issue is to use both solutions in a mix. One more filter is applied at each side of the PO-range, with the same spacing between each of the seven filters as for the previous five. Based on the original gain information for the seven filters, similar to the five showed by the blue curve in Figure 4.5 each filter gain is adjusted. The red curve is more uniform, though not constant, overall gain is achieved. The overall value of the gain is designed to be around 6 dB with the help of response plots. This is because the phase shift of the filters will cause some of the responses to add negative gain, which is not captured in the gain diagram. The phase diagram also clearly show a more uniform response, though there are still notable ripples, added phase for low frequencies and decreased phase for high frequencies. The variance is between 0.85 and 1.3 for the gain and ± 23°for the phase after adjustments have been made. This impact will be passed to the final output, but is deemed acceptable for this thesis. To mitigate the ripple effect seen in both plots the amount of parallel band-pass filters inside the range could be increased.

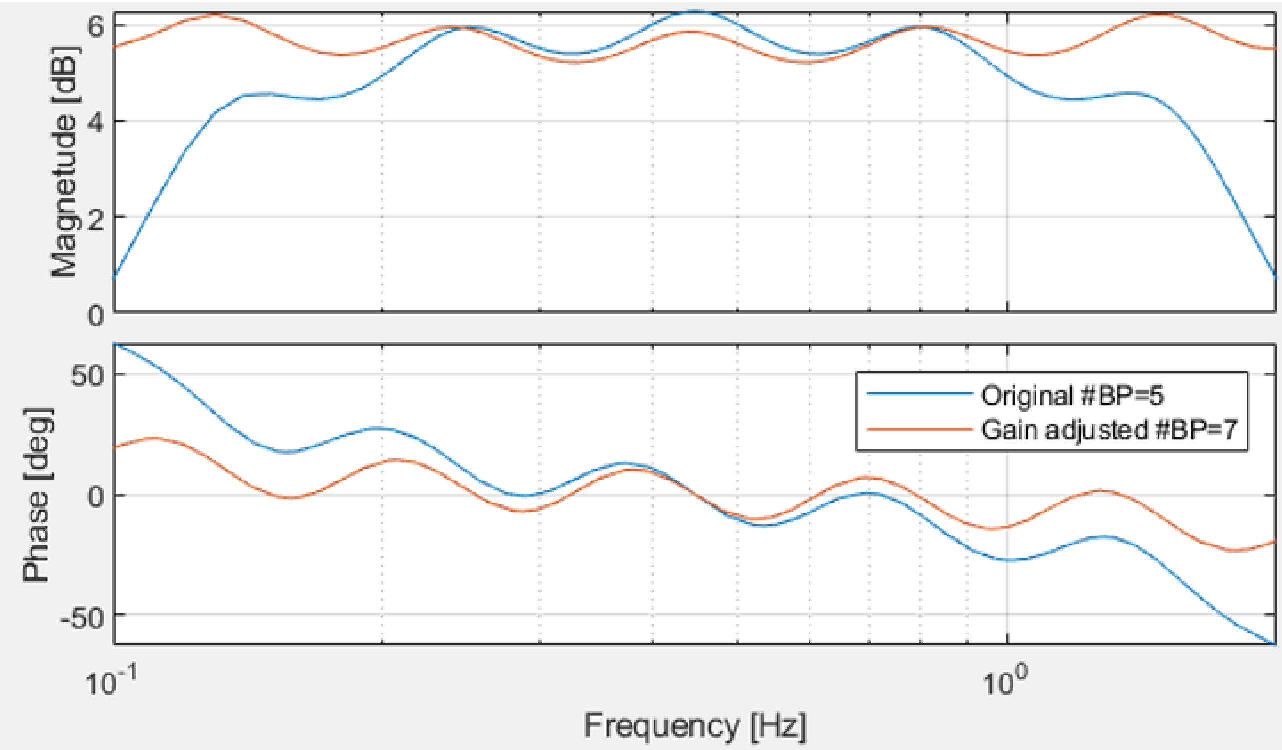

Figure 4.5: Bode plot of the summed output of the band-pass filters in the PO-frequency spectrum. Blue line is summation of responses from the 5 filters. Red line is proposed solution with 7 filters and adjusted gains to raise the gain of the outer filters.

4.2 Controller design

The POD-controller it self consists of two consecutive lead compensators. The first one compensates for the phase shift introduced by the measurement delay. The second compensates for the magnitude and phase shift of the wind turbine response. As explained in Chapter 3 the phase shift of both the delays and the WTG response depends on the frequency of the PO.

After calculating damping of the WTG and phase shift of both delays and WTG response, the lead-regulators are designed using the following equations:

$$G_{lead} = k \cdot \frac{a \cdot \tau_{G.lead} \cdot s + 1}{\tau_{G.lead} \cdot s + 1} \tag{4.2}$$

$$a = \frac{-sin(\phi_{pm}) - 1}{sin(\phi_{pm}) - 1} \tag{4.3}$$

$$\tau_{G.lead} = \frac{1}{\sqrt{a} \cdot \omega} \tag{4.4}$$

where ϕ_{pm} is the wanted phase margin of the lead regulator defined by $\phi_{pm} = 180 - \phi$. The gain, k of a lead regulator in this form is usually $\frac{1}{\sqrt{a}}$ to achieve a 0 dB gain at the design frequency, but as the response of the WTG introduces frequency dependant damping of the signal the gain is adjusted to also compensate for the damping defined in (3.4). Thereby k is defined as

$$k = \frac{\frac{1}{\zeta_{WTG}}}{\sqrt{a}} = \frac{\frac{1}{\left|\frac{1}{\tau_{WTG} \cdot j \cdot \omega_{PO} + 1}\right|}}{\sqrt{a}} \tag{4.5}$$

The phase shift capacity of a lead regulator is at maximum 90 °, since there is only one zero in the transfer function. Realistically, the hardware components will limit the practical achievable limit to about 70°[27, sec: 6.3]. So even though $\phi_{pm.max} = \phi_{Delay.max} + \phi_{WTG.max} = 85.5$ is under the theoretical limit, the phase compensation for WTG and delays are split into two series connected lead regulators. As a design example, a lead regulator compensating for WTG response at an input frequency of 0.45 Hz (matching frequency of the fourth branch) is shown in Figure 4.6. Here the needed phase compensation is calculated from (3.3) to be 24.1°.

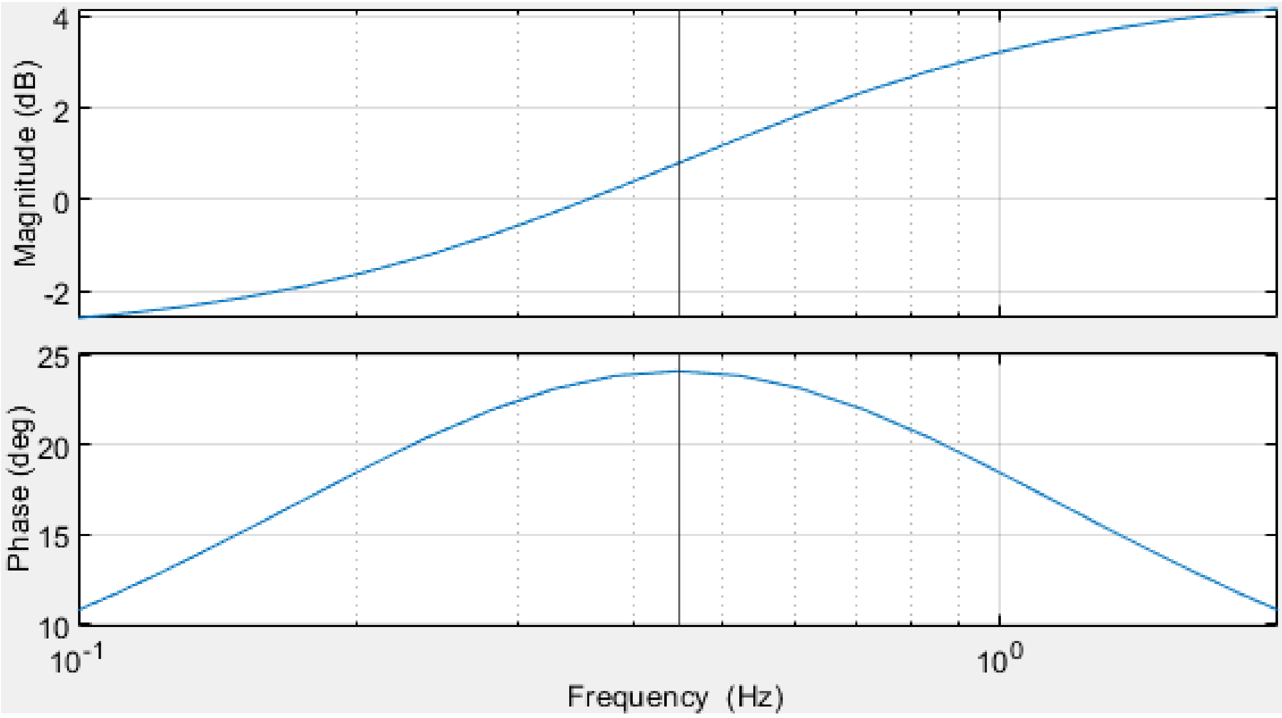

Figure 4.6: Bode plot of the lead regulator compensating for the phase shift caused by the WTG response for an input frequency of 0.45 Hz.

It is visible that the phase lift provided is indeed 24.1°and the magnitude at the design frequency is $\frac{1}{\zeta_{WTG}} = 0.79$ dB as the design criteria. One disadvantage of the lead regulator without a lag component is the high gain for frequencies over the design frequency. However, since the first order WTG response has a damping effect on higher frequencies, the high gain from the lead regulators is not as critical. In Figure 4.7 it is illustrated that for design frequency of 0.45 Hz, the high frequency gain of the lead regulator is minimized by the damping of the WTG response. Since the Bode plot for the WTG response is constant for all branches, but the response from band-pass and lead regulator varies with the design frequency, this will not have exactly the same curvature for other design frequencies. The original damping characteristics of the band-pass filter is still altered as frequencies lower than the design frequency have lower gain and frequencies just over the design frequency have slightly higher gain. However, the general concept that one part raises gain and the other damps at high frequencies is a general concern.

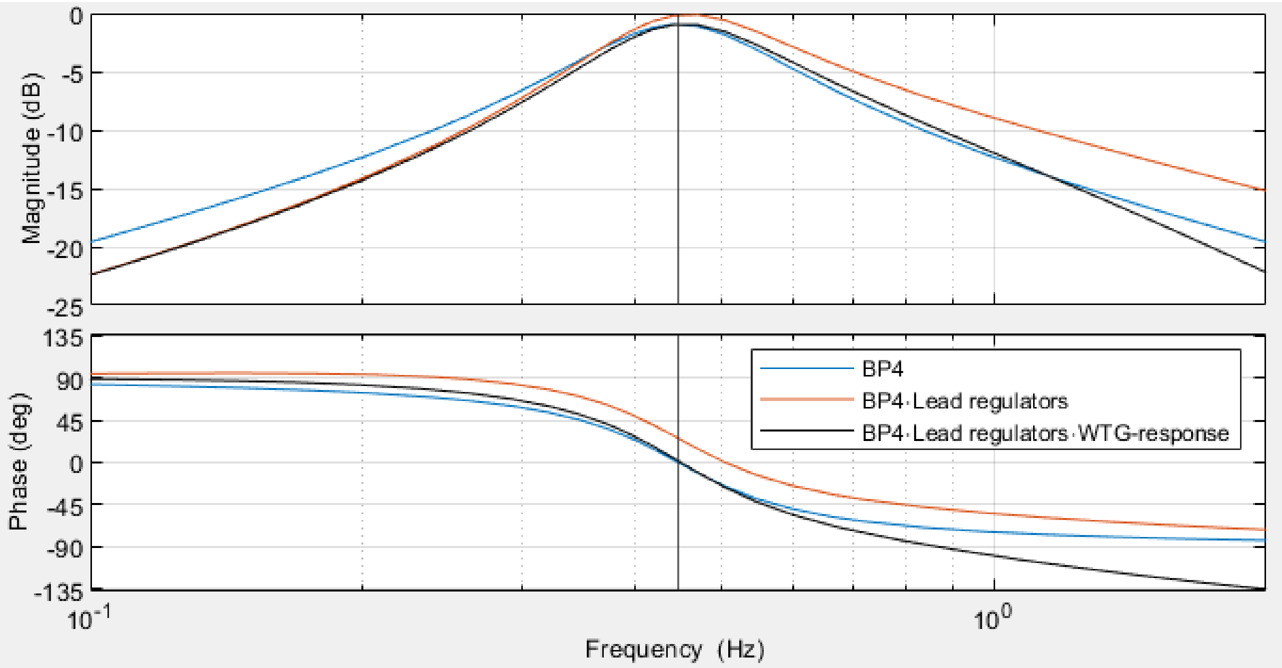

Figure 4.7: Bode plot to show that high frequency gain of the lead regulator is mitigated by the WTG response damping.

4.2.1 Communication delay considerations

In section 3.4 it was stated that phase shift from communication delay depends both on turbines position in the array and oscillation frequency. In order to compensate for communication delay using the strategy of parallel filter & controller branches increases the number of compensators significantly. The double frequency dependency causes the system to have nine different phase shifts for each parallel branch, i.e. 63 phase regulators are needed for the proposed design. A design including this many lead regulators is deemed both cumbersome and unrealistic to implement and therefore the analysis will instead compensate for the average communication delay, $T_{D.com.mean} =$ 11.5 ms in every parallel branch. The maximum phase error caused by this approximation is per (3.9)

$$\phi_{Delay.maxerror} = (T_{D.com.max} - T_{D.com.mean}) \cdot \omega_{max} = 9.2ms \cdot 2Hz \cdot 2\pi = 6.6^{\circ}$$

4.3 Open loop system response

With the band-pass filter and the lead regulators designed for seven parallel branches, the total response of the system can be investigated. With the diagram in Figure 4.8a the whole system dynamic presented in Figure 4.1 is shown. The input is a sinusoidal signal with the amplitude of 1. The measured input is the signal after measurements and the washout and low pass filters, then the signal pass through the band-pass filter of the fourth branch. The band-pass output passes through a lead regulator designed for the measurement delay, then through the lead regulator designed for WTG response and is now sent from controller to the WTG. The diagram is a snip of the response so it is easier to see the effect of delays, filters, lead regulators and the WTG response. It must be noted that the Compensated measurement, which is the input to the second regulator, is on top of the WTG output curve as the lead regulator compensated perfect for the WTG response at the design frequency.

(a)

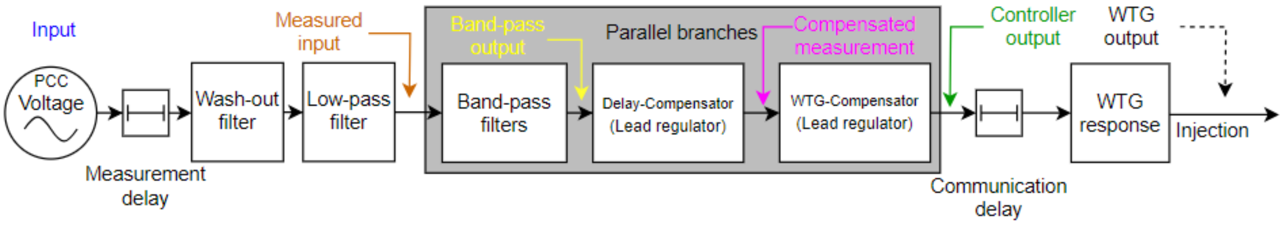

(b)

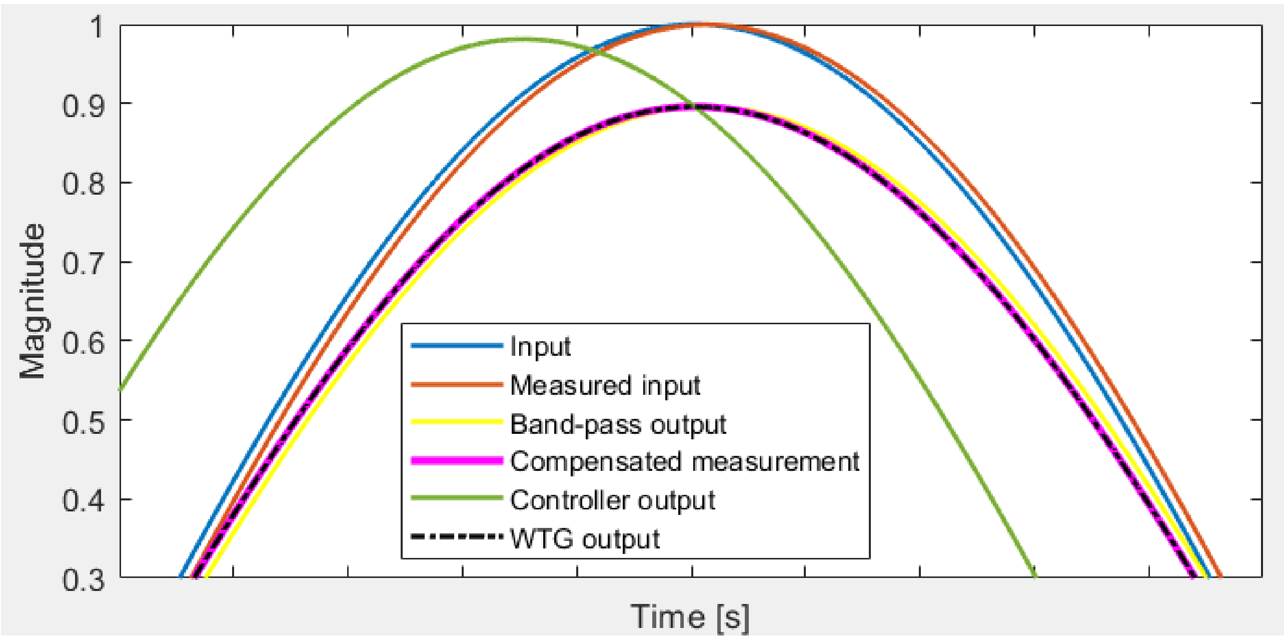

Figure 4.8: (a) Reprint of Figure 4.1 with explanation of where the signals of Figure 4.8b is measured, for convenience of the reader. The communication delay is set to 0 in the open loop design. **(b)** Time response plot of the whole branch 4.

For the full response of the POD controller, outputs of each filter-controller branch must be added together like they were for the band-pass filters in Figure 4.4. The input frequency is chosen at the minimum of the PO-range, 0.1 Hz, to investigate the phase shift at low frequency. As discussed in the filter design section 4.1, the outer frequencies within the range will be subjected to a phase shift from both the high and low pass filters and the parallel band-pass filters. Using the minimum frequency is chosen to analyse one of the border frequencies. In Figure 4.9, the response of the branches combined is shifted in phase to lead the input oscillation by 17°. This can be explained by the phase lift from the high and low pass $\phi_{HP-LP-0.1}$ and the phase lift from the band-pass filters $\phi_{BP-0.1}$. The black curve is the input oscillation minus the WTG output, since the POD controller would be implemented with a gain of minus one to flip the phase 180 °and counteract the measured signal. As seen by the magnitude of this curve, the POD controller can provide a signal that would damp the power oscillation. If ideal controllability and 1-to-1 power rating of grid versus power plant is assumed, the power oscillation of 0.1 Hz would be damped to around 30 % of the original magnitude.

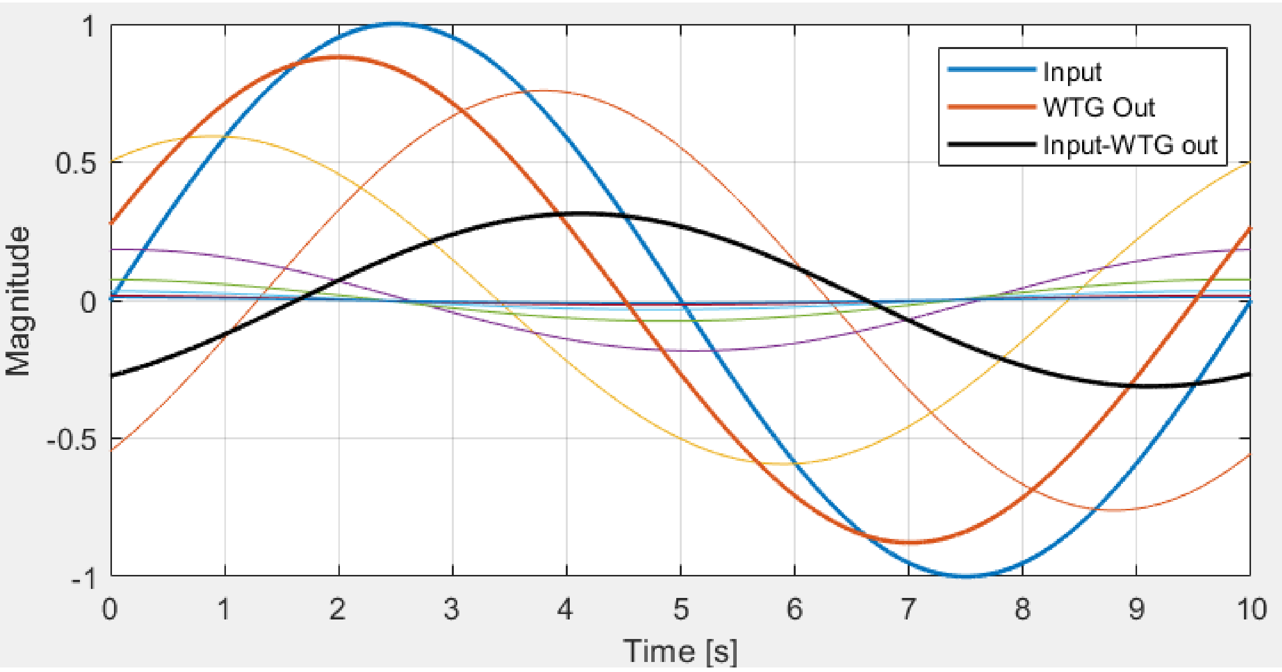

Figure 4.9: Time response for the control system. The WTG output is the total sum, which is plotted on top of the response for every individual branch.

With the table values of delayed phase in Table 4.1 it is clear that all but one band-pass filter contribute with negative phase delay, or phase lead, causing the final output to also be leading the input signal. However, mitigated by the uneven gain distribution, as the thin orange curve has higher gain than the yellow. Both their design frequencies are placed at the same distance from the input frequency.

Table 4.1: Phase and time delays of every signal in Figure 4.9 compared to the input signal.

Signal name	Time delayed [s]	Phase delayed [°]
Band-pass 1	1.3	46.4
Band-pass 2	-1.6	-58.0
Band-pass 3	-2.4	-86.4
Band-pass 4	-2.6	-94.3
Band-pass 5	-2.7	-98.3
Band-pass 6	-2.8	-100
Band-pass 7	-2.8	-101
WTG out	-0.5	-16.9
Input-WTG out	1.6	57.2

4.4 Summary

The proposed control system consists of a low-pass and wash-out filter, parallel band-pass filters and lead regulators, which acts to control a plant consisting of measurement delay and WTG response. The input to the control system is voltage at PCC and the output is reactive power production of one turbine. The goal of the controller design is to compensate for the dynamics of delay and WTG response so the output has the same frequency and opposite phase of the oscillating part of the input.

The oscillating part of the input is found with wash-out and low-pass filters designed at a cut of frequency one decade away from the PO-frequency limits of 0.1 and 2.0 Hz. This limits the phase shift to $\pm$ 5°and a neglectable damping. Parallel band-pass filters are designed to divide the PO-range into smaller ranges for more precise phase shift compensating by the lead regulators. Five band-pass filters are designed within the PO-range being logarithmic evenly distributed to cover the range. Through time response and Bode analysis it was, discovered that filters outside the range are needed as well as individual gain adjustment for each filter to achieve better phase performance for frequencies inside the defined range. Thereby, two filters are added outside the range on each side and all seven filter gains are adjusted so that the outer filters gains are higher than that of the inner filters. Though the effect is mitigated, the band-pass filters still add phase for low frequencies and decrease phase for higher frequencies spanning between $\pm$ 23°. The summed gain of the filters also varies with the frequency between 0.85 and 1.3 with lowest gain in the middle of the spectrum. For further uniform behavior, the amount of filters can be increased.

Two lead regulators are designed for each of the seven band-pass filters, one to compensate for WTG time response and one to compensate for delay introduced by measuring equipment. As the WTG response affects both magnitude and phase, the compensating lead regulator is designed with a gain to counteract the WTG damping and a phase lift which matches the WTG phase lag at the design frequency. The other regulator compensates for measurement delay and average communication delay. The average communication delay to the nine turbines in each array is 11.5 ms which is competed by the regulator. The maximum phase error introduced by using the average delay occurs when damping a 2 Hz signal and is 6.6°. Finally the time response of the filters, controller, measurement delay and WTG response is analysed to validate the design. It is found that the output signal leads the input for low frequencies and lags the input for high frequencies, with the design frequency for the middle filter matching exactly in phase. The amount of gain between input and output oscillates as the frequency changes as discovered in the band-pass analysis. However, with those variating factors the lowest PO-frequency (0.1 Hz) is analysed and the output still only leads the input by 17°and can thereby still have a damping effect.

5. Control verification in WPP

5.1 Test system setup

The electrical setup of Figure 2.1 with WPP, plant transformer and external grid connection is implemented in a Newton-Raphson load flow script [28]. In Figure 5.1 the reactive power setpoint calculated by the controller is fed into the WTG model, that calculates the active and reactive production and sends it to the network model. The network model conducts a load flow analysis and calculates the voltage at PCC, which is then measured and used as input to the control system.

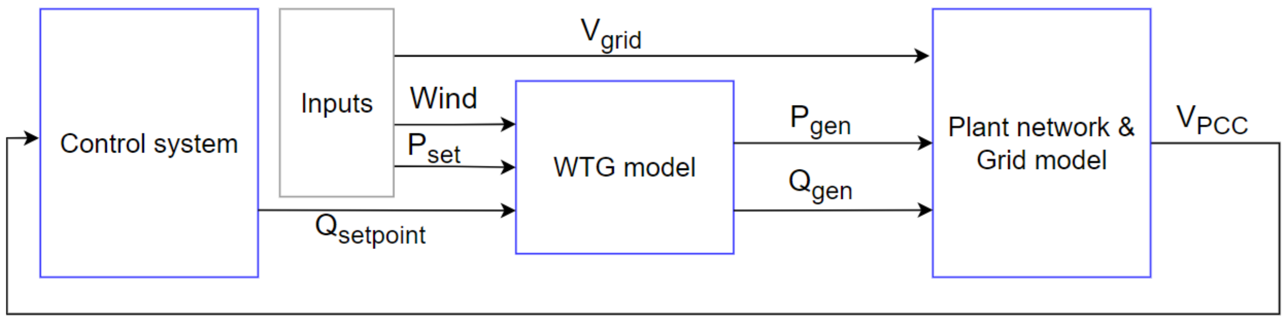

Figure 5.1: Interface between the control system developed and the externally developed models adapted to test the control system in closed loop.

As the communication delay is assumed to be equal for all turbines, the setpoints and thereby power generation is equal for all turbines. The injected power from the WTG model to the plant & grid model is therefore identical for all turbines, but dealt individually to each of the WTG connected busbars. The voltage at the external grid, V_{grid}, is an oscillation around 1 PU with 0.01 amplitude, where the frequency is controlled representing a power oscillation caused by power plants in the external grid.
In the WPP network setup, the external grid bus acts as a slack bus, where as the busbars connected directly to a turbine are configured as PQ-busses. General control of the wind turbine with regards to active power control and voltage slope control etc. is omitted to simplify the test setup. The active and reactive power setpoints are set to 1 and 0.2 respectively. Dynamics of varying wind profiles are also omitted why the wind is seen as a constant input of sufficient wind for 1 PU active power production.

5.2 Phase characteristics of WPP as POD device

To analyse the effect of the WPP cable network on the reactive power output, the sum of reactive power generated by the turbines is plotted along with reactive power injection at PCC. The difference in magnitude between the two depends on the non oscillating reactive power output of the turbines, which in this case is 0.2 PU, but the frequency and phase of the oscillation should be unaffected by this. By closely analysing Figure 5.2 a small phase shift of 3°is observed. Thereby the plant network impact on POD capabilities of the WPP is relatively low.

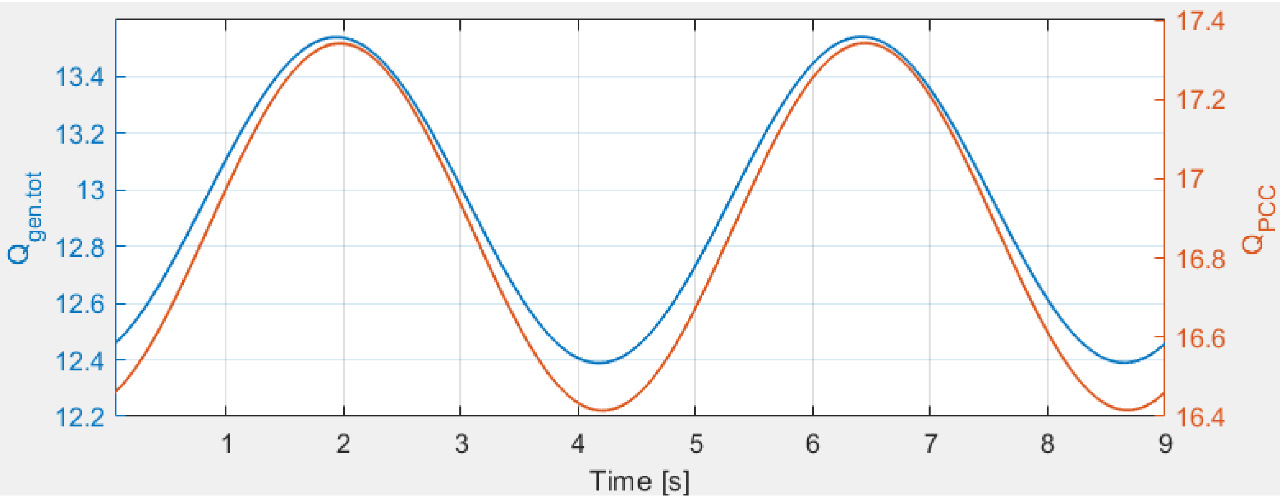

Figure 5.2: Comparison between the total reactive power produced by the turbines (Q_{gen}) and the reactive power injected at PCC (Q_{PCC}) for PO with 0.1 Hz. Q_{PCC} lags Q_{gen} by 3°. Two y-axis are used for the oscillations to be compared by their phase.

Figure 5.3 compares the voltage at point of common coupling to the injected reactive power for a PO frequency of 0.1 Hz. The reactive power injection at PCC is measured with no communication delay and no compensation as well as with variable delay and average delay compensation. Compared to the voltage, the reactive power output is turned 180°to counter act the voltage swings. Measuring the additional phase delay, it is found that the output is lagging the input by 20 °when no communication delay is included. This amount of phase shift is similar to the phase lead of 16.9°discovered in the control system analysis in Figure 4.9. If communication delay is included and the lead regulator compensates for the average delay, the phase lead moves to 19.5°.

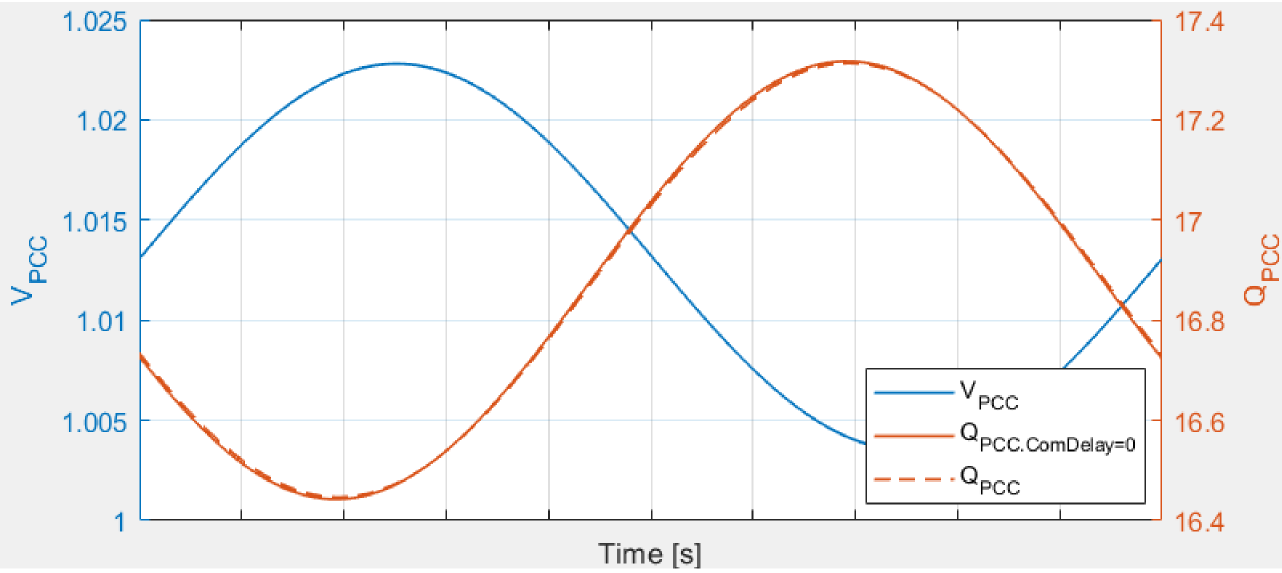

Figure 5.3: Comparison between the voltage at PCC and the reactive power injected to the PPC. Compared to the input, V_{PCC}, the phase delay of the outputs are 160°for $Q_{PCC.ComDelay=0}$ and 160.5°for Q_{PCC}.

The worst case input for the designed controller is at 2 Hz, since studies in chapter 4 showed high gain for high frequency and the phase shift due to communication delay is highest for 2 Hz input. As shown in Figure 5.4a, also the phase shift due to WPP network is higher for 2 Hz than for 0.1 Hz, as the phase shift in this case is 7 °, compared to the 3 in Figure 5.2. For the full response Figure 5.4b shows $Q_{PCC.ComDelay=0}$ lagging the input by 223°and Q_{PCC} lagging 230°, which means they are lagging the optimal phase by 43°and 50°respectively. The reason for this relative high phase lag at high frequencies is a combination of lead regulator gain, overall band-pass lag response, communication delay and WPP network phase shift. For the output reactive power to contribute towards damping of the voltage at PCC, the phase shift can however be up to 60°. Therefor, with design of just seven parallel branches, the proposed design meets the requirements.

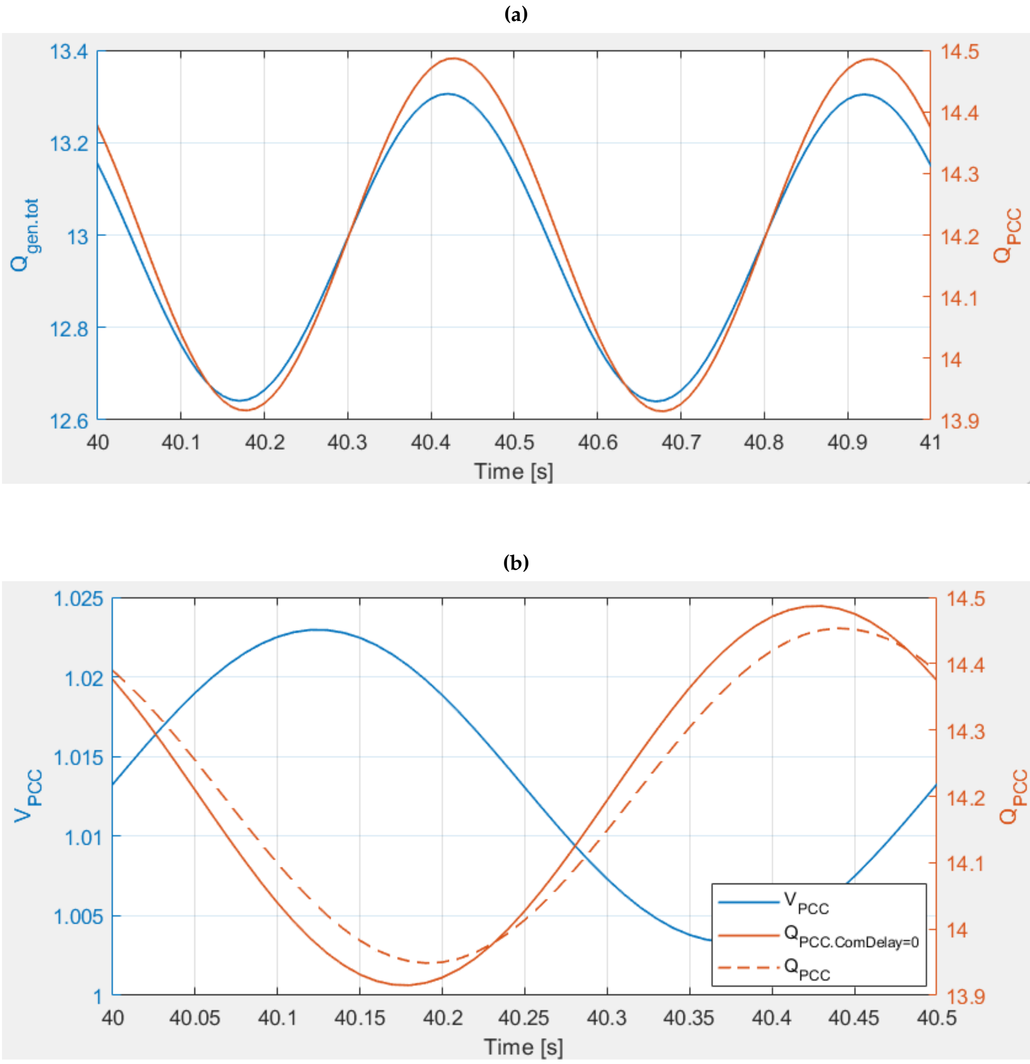

Figure 5.4: (a) Total reactive power produced (Q_{gen}) versus reactive power injected at PCC (Q_{PCC}) for PO with 2 Hz. Q_{PCC} lags Q_{gen} by 7°. **(b)** Comparison between the voltage at PCC and the reactive power injected to the PPC for 2 Hz input. Compared to the input, V_{PCC}, the phase delay of the outputs are 223°for $Q_{PCC.ComDelay=0}$ and 230°for Q_{PCC}.

These final tests for each border frequency proves that the developed controller is able to compensate adequately for delays and turbine response, thereby controlling the wind power plant to produce reactive power in opposite phase of the voltage measured at PCC and consequently assist in damping the observed power oscillation.

5.3 Summary

The control system is tested using a WTG model [20] and a plant network and grid model [28]. Using these models, the phase lag from the WPP internal network is found to be 3°, by comparing the total generated reactive power with the injection on PCC for an input frequency of 0.1 Hz. With the same input oscillation, the influence of the variable communication delay is analyzed. By comparing the reactive power injection at PCC with no communication delay to the injection with variable communication delay and average compensation, only a limited difference was found. Considering communication delay, the signal was found to be lagging 0.5°in comparison. The final reactive power output was found to have a phase lag of 160°from the voltage at PCC, meaning that for a input frequency of 0.1 Hz, the POD reactive power output is leading 20°compared to the ideal compensation. Findings in chapter 4 indicated that the worst case frequency for the controller is 2 Hz, suggesting further analysis of this specific input frequency. For 2 Hz oscillation, the WPP network creates a phase delay of 7°, and the communication delay simplification causes an additional phase lag of 7°. Due to these delays and those discussed in chapter 4, the reactive power produced are lagging 50°compared to the optimal phase. With the amount of phase shift in both these examples, it is still possible for the WPP to provide damping capabilities to the power system.

6. Discussion and Conclusion

6.1 Summary of work

This master thesis aimed to develop a power oscillation damping controller used for wind power plants. The actual damping capabilities of power oscillations in a power system depend on the topology of the electrical grid and the connection point of the damping device. Therefore, site specific grid models are needed to simulate the damping of a power plant and investigate optimal damping strategies. Current grid codes developed for power oscillation damping by wind power plants do not require any specified amount of damping, but rather that damping functionalities are in place. Therefore, a general interpretation of the grid has been used to design a controller which produces a damping signal opposite of the observed oscillation.

A system is defined for the controller to be implemented and tested in. Through system requirements a small wind power plants with two arrays of nine turbines each and a park transformer is defined and connected to an external grid represented by a Thevenin equivalent voltage source. The observation parameter for the POD controller is voltage measurement at the PCC. Through different grid meters on the market, the delay of measuring the voltage is estimated to 10 ms. Delays regarding communication from the PCC to the wind turbines are configured to be using hop-by-hop communication where the total delay is defined from the transport time between each turbine and the internal processing time in the turbine. The communication delay for the closest turbines is estimated at 2.3 ms whereas the furthest turbines have 20.7 ms of communication delay.

The turbine is modelled as a first order response with the WTG converter band-width of 1 Hz determining the response speed. It is investigated that with faster acting turbine response, the phase shift of frequencies in the PO-range can be massively decreased and the damping practically removed. Cables in the WPP are modelled using the π model and defined in length by typical distances between turbines in offshore plants and in size by the maximum passing current. Hence larger cables are used closer to the PCC where current from a larger amount of WTGs is passing through. The transformer is modelled by winding resistance and reactance, where the magnetization branch is neglected. The grid impedance of the Thevenin equivalent voltage source is defined to be a stiff grid by SCR parameterized at 30 and X/R-ration at 10. Furthermore, both measurement and communication delays are represented as continuous delays.

When the voltage is measured at PCC, it passes through a washout-filter and a low pass filter, to remove both higher frequency noise and steady state signals leaving only frequencies in the PO-range. To minimize influence on the PO signals, these filters are designed using cutoff frequency one decade away from the PO-range limits, which limits the phase shift to under 5°. Further distinguishing between signals inside the range are made with seven parallel band-pass filters placed before the phase regulators. Because the phase shift depends on the oscillation frequency, this allows the phase regulators to be tuned for seven different phase shifts giving the controller a better performance throughout the PO-range. The band-pass filters introduce a nonlinear phase shift since their operating areas overlap and the middle ones have more neighbouring filters. To mitigate the nonlinear phase shift from the band-pass filters, the gains of each filter are adjusted, so the outer filters have a higher gain than the middle ones as well. Moreover, one filter is placed with a design frequency outside the PO-range on both sides. However, this non linear gain and phase characteristics of the band-pass filters are not completely eliminated and phase shift of up to 25°is introduced at the PO-range limits. The output of each band-pass filters passes to lead regulators compensating for phase shifts caused by delays and both damping and phase shift of the turbine response. For the compensation of WTG response, the phase margin of the lead regulators are designed to lift the phase the exact amount of degrees which the turbine response lags its input for each of the seven different design frequencies. Also the frequency dependent WTG damping of the signal is compensated by adjusting the gain of each lead regulator.
By analysing the control system time response including filters, controller, measurement delay and WTG response simulations illustrated that the designed controller is capable of producing an output signal with the same frequency and opposite phase characteristics as its input. Furthermore graphs showed how delays and WTG response influence the signal, and how the regulators compensate to keep the signal unaffected. Despite dividing input frequencies in several groups to enhance the performance for all frequencies, the designed POD controller has its best performance in the logarithmic middle of the range. However, due to the adjusted gains of the band-pass filters, the controller output only has a phase error of 18°at the lowest frequency in the range (0.1 Hz). Though it is not optimal, with such small phase error, the control can still have damping effects on the power oscillation.

Lastly, the controller is verified on the full system setup using load flow simulation to calculate the power flow in the WPP network with the connected external grid. Externally developed models for WTG and load flow calculations are adapted to fit the analysis of this project and the controller output is fed into the WTG model as an addition to the reactive power setpoint. For the load flow calculations the power production from turbines is fed into the PQ-busbars. By comparing the total WTG reactive power production with the reactive power injected at PCC, it is found the the cables and transformer causes a phase lag of around 3°. With this added small phase shift the WPPs full ability to provide reactive power in the opposite phase of the voltage is shifted by under 20°for a scenario of damping a 0.1 Hz power oscillation. For the 2 Hz, i.e. the highest PO-frequency, the phase lag between generated power and injected power at PCC is 7°as also the phase lag from communication delay is an extra 7°. These phase shifts along with the high frequency lead regulator gain, causes the reactive power output to be lagging the optimal damping by 50°. With the phase shift in both these examples, the reactive power output to the PCC can still be considered to contribute positively to the damping capabilities of the power system.

6.2 Recommendations

This thesis found that estimating important parameters as communication delay, measurement delay and WTG response time have a very significant impact in the controller design. When the uncertainty of parameter estimation has a factor of ten as presented in chapter 2 different estimations can dictate the design. As an example, a ten times faster WTG response will result in practically no damping within the frequency range and maximum phase shift at just 10°as opposed to more than 60°used in this thesis. On the contrary, when estimating the communication delay a ten times slower communication speed was discussed. If these are the communication delays of the POD WPP, the strategy proposed in this thesis of using the average communication delay would cause serious phase delays, and would not be an acceptable strategy. The communication delay variance was in this thesis determined by the hop-by-hop communication strategy, which again would change the communication delay variance if a different strategy was applied. In general, POD control will have its best prerequisites in a system with low measurement delay, low WTG response time and especially low variable communication delay.

In normal PSS structure, for both single and multi-band, the common control structure utilizes one or more lead-lag controllers [29] to control the phase characteristics from input to output. As POD functionalities are based on the well developed and tested PSS structure, the lead-lag is mostly used for POD by WPPs. However, the findings in this thesis by utilizing parallel controller branches challenges the standard phase control structure. The lead regulator can compensate for the phase shift at the design frequency but will always have a larger gain at the frequencies above the design frequency, which is usually handled by a lag regulator. When the damping from the wind turbine response increases with the frequency it was found that the increased gain from lead regulators is reduced by the damping from the WTG response. Since the gain of lead regulators is determined by the amount of phase needed to compensate for the WTG response, this effect will be true even if a faster or slower WTG response time is used.

It is recommended that grid operators and grid code developers setup quantified values for maximum phase shift between the power oscillation at the accessible PCC and the POD output of the wind power plant. As presented in this thesis, a POD controller must be expected to have some undesirable phase shift between the input and output, at least for some frequencies inside the range. This is also allowed by the few grid codes addressing POD from WPPs. However, when the grid codes only state that power oscillation functionalities must be in place it does not ensure quality in the developed control, and the control developer must determine the acceptable level them selves. As discussed an actual level of contributed damping is an unrealistic requirement, since testing of this would require either extensive modelling or can only be done when the plant is already implemented on site. The suggestion of specifying a maximum phase deviation from the POD functionality would provide an acceptance criteria for the control design that is easily testable with simple models of just the power plant equipment. These tests can be done with models probably already used by the plant operator for test of various grid codes and internal plant requirements.

6.3 Future work

To continue developing and validating the POD design framework presented in this thesis, a few interesting areas are listed below:

- **Validation of input filters.** The low pass filter and washout filter in the designed control system are included to exclude all non power oscillation frequencies from the measured signal. However, in this design they have not been designed against any expected power system signals that might compromise the signal quality. For a thorough filter design, the input could either be a real power system measurement or an estimation including common frequencies related to interharmonics, subharmonics, switching, dc gain variations and more. An analysis like this might lead to a more aggressive or more conservative design, which in the end will have an impact on the phase characteristics within the PO-range.

- **Power oscillation representation.** The power oscillations have been represented by sinusoidal signals with no damping in this thesis. Realistically, the power oscillations will have some amount of damping from PSS or other POD devices in the external grid. A more accurate representation of the power oscillations measured at PCC could include a damping factor and magnitude matching one or more of the power oscillation events previously detected in the European power system as mentioned in section 1.2. An analysis using a more accurate power oscillation input could also study a time frame of how fast the POD controller should produce the damping signal after the power oscillation is visible at PCC.

- **Discretization of filters and controller.** When the POD controller is to be implemented as part of the power plant control it needs to be discretized. As for all discretization this might cause the designed control to change for critical frequencies and in worst case be unstable depending on the method used. The low pass and washout filters can be assumed to be analog, but band-pass filters should be implemented digitally along with the controller, so they can be tuned together. Preliminary comparisons between discretization methods showed that the Tustin method have a better fit in Bode plots than the Least-square and basic zero-order-hold methods. For the complete discretization, however, other methods should also be considered and poles should be tracked to ensure a stable system design.

- **Combination with general WPP controller.** The POD controller should be tested along other WPP controller functions as voltage control as well as it should be objected to variable wind conditions. Several complications can be identified with such analysis. If the voltage controller demands maximum reactive power output from the WPP, there will be no possibility of providing POD-Q as well, which dictates that a prioritization between different control functions must be made. This prioritization must be made with regards to the grid codes and in some cases direct collaboration with the affected TSO.

References

[1] Andrzej Adamczyk. *Damping of Low Frequency Power System Oscillations with Wind Power Plants*. Tech. rep. 2012. URL: http://www.et.aau.dk.

[2] Graham Rogers. *Power System Oscillations*. Boston : Kluwer Academic, 2000. ISBN: 0792377125.

[3] Sen Gupta and Indraneel Sen. *Low frequency oscillations in power systems: A physical account and adaptive stabilizers*. Tech. rep. 5. 1993, pp. 843–856.

[4] entso-e. *European Network of Transmission System Operators for Electricity ANALYSIS OF CE INTER-AREA OSCILLATIONS OF 19 AND 24 FEBRUARY 2011 ENTSO-E SG SPD REPORT*. Tech. rep. 2011. URL: www.entsoe.eu.

[5] entso-e. *European Network of Transmission System Operators for Electricity ANALYSIS OF CE INTER-AREA OSCILLATIONS OF 1 ST DECEMBER 2016 ENTSO-E SG SPD REPORT*. Tech. rep. 2017. URL: www.entsoe.eu.

[6] entso-e. *Oscillation Event 03.12.2017 System Protection and Dynamics WG*. Tech. rep. 2018.

[7] Prabha Kundur. *Power System Stability and Control*. McGraw-Hill, 1993. ISBN: 0-07-035958-X.

[8] Prasenjit Dey, Aniruddha Bhattacharya, and Priyanath Das. "Tuning of power system stabilizer for small signal stability improvement of interconnected power system". In: *Applied Computing and Informatics* 16.1-2 (Dec. 2017), pp. 3–28. ISSN: 22108327. DOI: 10.1016/j.aci.2017.12.004.

[9] entso-e. *Network Code for Requirements for Grid Connection Applicable to all Generators This document reflects the work done by ENTSO-E in line with the ACER Framework Guidelines on Electricity Grid Connections*. Tech. rep. 2013. URL: www.entsoe.eu.

[10] Energinet. "Energinet_kravanmeldelse-rfg-december-2022-uden-mark-up". In: (2022).

[11] Energimarknadsinspektionen. *EIFS2018:2 -Energimarknadsinspektionens föreskrifter om fastställande av generellt tillämpliga krav för nätanslutning av generatorer*. Tech. rep. 2018.

[12] Lennart Petersen et al. *Addressing Power Oscillations Damping Requirements for Wind Power Plants*. Tech. rep.

[13] Samundra Gurung et al. "Optimized tuning of power oscillation damping controllers using probabilistic approach to enhance small-signal stability considering stochastic time delay". In: *Electrical Engineering* 101.3 (Sept. 2019), pp. 969–982. ISSN: 14320487. DOI: 10.1007/s00202-019-00833-6.

[14] Jiajun Nan et al. "Wide-area power oscillation damper for DFIG-based wind farm with communication delay and packet dropout compensation". In: *International Journal of Electrical Power and Energy Systems* 124 (Jan. 2021). ISSN: 01420615. DOI: 10.1016/j.ijepes.2020.106306.

[15] Bachmann electronic GmbH. *GM260 - Grid Measurement Module*. Tech. rep. 2021.

[16] Bachmann electronic GmbH. *GMP232/x - Grid Measurement and Protection Module*. Tech. rep. 2022.

[17] Beckhoff. *EL34xx - 3-phase energy and power measurement terminals*. Tech. rep. 2022.

[18] Mohamed A. Ahmed and Young Chon Kim. "Communication network architectures for smart-wind power farms". In: *Energies* 7.6 (2014), pp. 3900–3921. ISSN: 19961073. DOI: 10.3390/en7063900.

[19] Mohamed A. Ahmed and Chul Hwan Kim. "Communication architecture for grid integration of cyber physical wind energy system". In: *Applied Sciences (Switzerland)* 7.10 (Oct. 2017). ISSN: 20763417. DOI: 10.3390/app7101034.

[20] Lennart Petersen et al. "Validating performance models for hybrid power plant control assessment". In: *Energies* 12.22 (Nov. 2019). ISSN: 19961073. DOI: 10.3390/en12224330.

[21] Richard J.A.M. Stevens et al. "Combining economic and fluid dynamic models to determine the optimal spacing in very large wind farms". In: *Wind Energy* 20.3 (Mar. 2017), pp. 465–477. ISSN: 10991824. DOI: 10.1002/we.2016.

[22] Hadi Saadat. *Power System Analysis*. Ed. by Mary K. Coman. Second Edition. McGraw-Hill Higher Education, 2002. ISBN: 0-07-284796-4.

[23] ABB. *XLPE Submarine Cable Systems Attachment to XLPE Land Cable Systems-User ́s Guide Rev 5 2 XLPE Submarine Cable Systems | ABB*. Tech. rep. 2010. URL: www.abb.com/cables.

[24] J.Duncan Glover, Mulukutla S. Sarma, and Thomas J. Overbye. *Power System Analysis and Design*. 5th ed. Vol. 850. Global Engineering, 2012. ISBN: 978-1-111-42579-1.

[25] Hangzhou Qiantang River Electric Group. *120MVA 132kV 3-phase 2-winding Power Transformer with OCTC*. Tech. rep. URL: https://www.qretransformer.com/132kv-power-transformer/57280758.html.

[26] Hank Zumbahlen. *Linear Circuit Design Handbook*. 2008.

[27] Kamran Iqbal. *INTRODUCTION TO CONTROL SYSTEMS*. LibreTexts. URL: https://LibreTexts.org.

[28] PG Praviraj. *Newton-Raphson Loadflow*. Aug. 2023. URL: https://se.mathworks.com/matlabcentral/fileexchange/21059-newton-raphson-loadflow.

[29] IEEE. *IEEE Std 421.5-2016: Recommended Practice for Excitation System Models for Power System Stability Studies.* IEEE, 2016. ISBN: 9781504408554.

A. Component parameters used for modelling

Table A.1: Selected cables corresponding to the maximum current through their connection. The cables are identical for the two parallel arrays.

Connection	Max current $I_{cable.max_N}[A]$	Cable rated current [A]	Cable Cross section $[mm^2]$
WTG9-WTG8	73	300	95
WTG8-WTG7	147	300	95
WTG7-WTG6	220	300	95
WTG6-WTG5	294	420	185
WTG5-WTG4	367	420	185
WTG4-WTG3	441	530	300
WTG3-WTG2	514	590	400
WTG2-WTG1	588	655	500
WTG1-BUS3	661	715	630

Transformer model	S11-120000/132
Transformer rating S_{nom}	120 MVA
Copper loss P_{copper}	337 kW
Short circuit impedance Z_{sc}	12-14 %
Resistance R_{tr}	$\frac{P_{copper}}{S_{nom}} = 0.003$ p.u.
Reactance X_{tr}	$\sqrt{Z_{sc}^2 - R_{tr}^2} = 0.12$ p.u.

Table A.2: Transformer parameters from a QRE (Quintang River Electric) transformer [25]